ENCLOSURE 8

MFN 09-552

NEDO-33173, Supplement 2, Part 3

Non-Proprietary Version

IMPORTANT NOTICE

This is a non-proprietary version of NEDC-33173P, Supplement 2, Part 3, from which the proprietary information has been removed. Portions of the enclosure that have been removed are indicated by an open and closed bracket as shown here [[ ]]

GE Hitachi Nuclear Energy

NEDO-33173
Supplement 2 Part 3
Revision 0
Class I
DRF 0000-0012-1297
DRF Section 0000-0103-8228-R0
August 2009

Non-Proprietary Information

Licensing Topical Report

Applicability of GE Methods to Expanded Operating Domains –

Power Distribution Validation for Cofrentes Cycle 15

INFORMATION NOTICE

This is a non-proprietary version of the document NEDC-33173P, Supplement 2, Part 3, which has the proprietary information removed. Portions of the document that have been removed are indicated by an open and closed bracket as shown here [[ ]].

IMPORTANT NOTICE REGARDING THE CONTENTS OF THIS REPORT

Please Read Carefully

The information contained in this document is furnished for the purpose(s) of obtaining NRC approval of the "Applicability of GE Methods to Expanded Operating Domains - Revision 2." The only undertakings of GEH with respect to information in this document are contained in contracts between GEH and participating utilities, and nothing contained in this document shall be construed as changing those contracts. The use of this information by anyone other than those participating entities and for any purposes other than those for which it is intended is not authorized; and with respect to any unauthorized use, GEH makes no representation or warranty, and assumes no liability as to the completeness, accuracy, or usefulness of the information contained in this document.

TABLE OF CONTENTS

LIST OF TABLES

LIST OF FIGURES

Abbreviations And Acronyms List

Term	Definition
BOC	Beginning of Cycle
BWR	Boiling Water Reactor
BWREDB	Boiling Water Reactor Engineering Data Bank
CFR	Code of Federal Regulations
CPR	Critical Power Ratio
CR	Control Rod
EOC	End of Cycle
Exp	Exposure
GE	General Electric Company
GEH	GE Hitachi Nuclear Energy
GENE	GE Nuclear Energy
GETAB	General Electric Thermal Analysis Basis
GNF	Global Nuclear Fuel
LHGR	Linear Heat Generation Rate
LPRM	Local Power Range Monitor
LTR	Licensing Topical Report
MCPR	Minimum Critical Power Ratio
Meas	Measured
MOC	Middle of Cycle
NRC	Nuclear Regulatory Commission (USA)
RMS	Root Mean Square
S.E.	Safety Evaluation
SLMCPR	Safety Limit Minimum Critical Power Ratio
SRSS	Square Root of the Sum of Squares
TIP	Traversing In-core Probe
USNRC	United States Nuclear Regulatory Commission
Wt	Weight

ABSTRACT

Gamma scans are non-destructive method to determine the relative fission product inventory in nuclear fuel. A gamma scan of fifty fuel assemblies was completed in 2005 at the Cofrentes nuclear power station. Because of measurement problems, data for only forty-six fuel assemblies are included in the report. The agreement between the measurements and predictions using the TGBLA06 lattice physics code and the PANAC11 BWR core simulator is excellent, with bundle RMS errors less than 2.3%. The data validate the applicability of lattice power distribution uncertainties for modern BWR core and fuel designs, as well as for current operational strategies. Cofrentes (La Central Nuclear de Cofrentes) is a high power density (58.6 kW/l) BWR/6 in Valencia, Spain that was operating at an uprated licensed thermal power for the period in which the current data were taken. Cofrentes was uprated 2% in 1988, another 2.2% in 1998, 5.6% in 2002 and 1.9% in 2003, taking it to 112% of original capacity, as summarized in the power-flow map below. The data points represent the off-line core tracking cases run for Cycles 13 and 15.

[[

]]

1. INTRODUCTION

1.1 OVERVIEW

Power distribution validation data for operating boiling water reactors is routinely taken in the form of traversing in-core probe (TIP) measurements. In this case, the average power of the four bundles surrounding the instrument tube is detected via a neutron sensitive or gamma sensitive detector. For potentially greater resolution and at greater effort and cost, gamma scanning is an independent, non-destructive method to determine the relative fission product inventory in nuclear fuel. Gamma scan measurements for the purpose of power distribution validation may be made on either bundle average or pin-by-pin measurements.

The subject of this document is bundle gamma scan measurements made at the Cofrentes nuclear power station in 2005 at the end of cycle 15B (EOC15B). Fifty bundles were scanned. Of these fifty bundles, four were eliminated from the database due to operator error during the measurement campaign (a required additional absorber in the beam was missing). The Cofrentes 2002 bundle gamma scan is documented in Reference 4.

1.2 GAMMA SCAN MEASUREMENTS

Gamma scan programs vary by specification of the physical locality of the measurement, time of performing the measurement, measuring time, and number of measurements. For example, the technique for measurements of "power" calls for detection of the 1.6 MeV gamma ray that accompanies beta decay of ^{140}La with a half-life of 40.2 hours. ^{140}La accumulates in fuel mainly from the beta decay of the fission product ^{140}Ba that has a half-life of 12.8 days. After about 10 days following reactor shutdown, ^{140}La is proportional to the ^{140}Ba atom density and decays with the ^{140}Ba half-life. The ^{140}Ba distribution in fuel is characteristic of the fission distribution or integrated power history over the last 5 half-lives or approximately 60-120 days of reactor operation.

Thus, the scan results can be used to determine "recent" core power distribution. The 12.8 day half-life of ^{140}Ba also makes it imperative that the gamma scan data be collected as soon as possible after core shutdown usually during refueling operations since bundles with powers of interest are normally reinserted for additional use. Spectral lines from other isotopes may be measured using specific techniques and target fuel conditions for the determination of plenum fission gas (^{85}Kr) and/or fuel exposure (^{137}Cs/^{144}Pr), however, power comparisons are the sole subject of this report.

1.3 ANALYSIS / COMPARISONS

A comparison of the measured ^{140}Ba distribution with predictions using the analytical tools of GNF (i.e., TGBLA/PANACEA) constitutes a validation of methods that may be used for methods licensing or determination of other licensing uncertainties. The "Improved Steady-State Methods," also known as TGBLA06 / PANAC11, for core design, licensing, and core monitoring (Reference [1]) are the current GNF methods; this methodology is examined in this report.

The general procedure used to compare to the measured gamma scan data include the following elements. First, the power/flow history of the core is input to the nodal simulator. During this process, the TIP predictions from the core tracking may be compared to the measured TIP response for the first phase of the power distribution validation process. The second step is to integrate the power history over the last 60-120 days of operation to generate the predicted nodal relative and pin-by-pin ^{140}Ba concentrations.

The final step is to statistically compare the experimental and predicted ^{140}Ba predictions and explain the relationships on a bundle, nodal, and axial basis. This process may also be repeated using the measured 6 inch average TIP readings that may be input to the adaptive methodology described in References [2] and [3] for consistent confirmation of SLMCPR uncertainties.

2. SUMMARY OF DESIGN CALCULATIONS

This document provides summaries of the comparisons of design calculations of ^{140}Ba with measured ^{140}La as a means of demonstrating the GNF capabilities for calculating nodal powers using TGBLA06 / PANAC11. The older methodology (TGBLA04 / PANAC10) is no longer used in domestic core monitoring or design efforts. There are two analytic approaches summarized herein for predicting the nodal ^{140}Ba. These include:

- The standard off-line TGBLA06 / PANAC11 non-adapted models used in GNF applications for reload design and licensing (off-line);
- The standard on-line TGBLA06 / PANAC11 application used in 3DMonicore™ with TIP and LPRM shape adaptation for on-line monitoring (adapted off-line).

2.1 NODAL AND BUNDLE COMPARISONS

For both of these analytic approaches, the nodal power distributions from the PANAC11 core tracking are post processed to produce the nodal ^{140}Ba distributions as described in Section 4.1 of Reference 4.

2.1.1 Statistical Comparisons

Comparisons between the (normalized) predicted ^{140}Ba distributions with the (normalized) measured ^{140}La distributions demonstrate that the uncertainties in the predictions are significantly less than the uncertainties used for power distributions in the GNF calculation process used in support of licensing calculations.

Fifty bundles were scanned. Of these fifty bundles, four were eliminated from the database due to operator error during the measurement campaign. These four bundles were [[ ]]. This leaves forty-six bundles.

For the gamma scan measurements, the estimated experimental uncertainty is [[ ]]for nodes 2-24 (see Section 2.2). The nodal gamma scan RMS between the gamma scan measurements and the PANAC11 based calculation of the nodal ^{140}Ba distributions ranges from [[ ]], depending on how many fuel assemblies are included and whether non-adapted or TIP and LPRM adaption is used to produce the nodal ^{140}Ba distributions (see next sub-section).

This compares to the value of value of [[ ]]for nodal RMS value for the last TIP set near the end of cycle for the off-line PANAC11 (non-adapted TIPs) compared to the measured gamma TIPs, as documented in Appendix A.

These results further confirm the use of the TIP comparisons for routine assessment of the performance of the PANAC11 based on-line monitoring and off-line design calculations.

2.1.2 Summary of Bundle / Axial / Nodal Comparisons

Table 2-1 summarizes statistical comparisons for the bundle, axial, and nodal components for the PANAC11 model.

The first three rows of data provide results when all 46 Gamma Scan fuel assemblies are included in the comparison. Eliminating two bundles on the outer peripheral locations results in only 44 fuel assemblies, as shown in the next two rows of Table 2-1. Eliminating three additional near peripheral fuel assemblies results in only 41 fuel assemblies in the database (See Section 9.2 for details).

Table 2-1 Summary of Bundle / Axial / Nodal Comparisons – PANAC11 vs. Gamma Scan

Core Tracking	Weighting	Number of Bundles	Bundle RMS	Bundle SIGMA	Axial RMS	Axial SIGMA	Nodal RMS	Nodal SIGMA	Case
Non-adapted	Octant	46	[[						Four Operator Error Bundles Removed
Non-adapted	Unit	46							Four Operator Error Bundles Removed
TIP and LPRM Adapted	Unit	46							Four Operator Error Bundles Removed
Non-adapted	Unit	44							Two Peripheral Bundles Removed
TIP and LPRM Adapted	Unit	44							Two Peripheral Bundles Removed
Non-adapted	Unit	41							3 near peripheral and 2 peripheral Removed
TIP and LPRM Adapted	Unit	41						]]	3 near peripheral and 2 peripheral Removed

3. SUMMARY OF [[ ]]

3.1 DEFINITION OF STATISTICS

As described in the SLMCPR methodology, a gamma scan affords insight into the [[

]]. The difference between the bundle prediction and measurement yields this insight. This particular uncertainty has been the subject of recent communications with the NRC.

In each four-bundle set, the [[ ]] is computed as

[[ ]]

where P_j is the bundle-integrated ^{140}Ba for bundle j. Therefore, in terms of the normalized gamma scan data or prediction,

[[ ]]

3.2 [[ ]] SUMMARY

The summary of [[ ]] is provided in Table 3-1.

Table 3-1 Summary of [[ ]] Statistics

Core Tracking	Weighting	Number of Bundles	Number of 4 Bundle Sets	RMS	SIGMA	Note
Non-adapted	Octant	46	9	[[		Four Operator Error Bundles Removed
Non-adapted	Unit	46	9			Four Operator Error Bundles Removed
TIP and LPRM Adapted	Unit	46	9			Four Operator Error Bundles Removed
Non-adapted	Unit	44	8			Two Peripheral Bundles Removed
TIP and LPRM Adapted	Unit	44	8			Two Peripheral Bundles Removed
Non-adapted	Unit	41	8			3 near peripheral and 2 peripheral Removed
TIP and LPRM Adapted	Unit	41	8		]]	3 near peripheral and 2 peripheral Removed

4. PLANT AND FUEL DESCRIPTION

Cofrentes (La Central Nuclear de Cofrentes) is a high power density (58.6 kW/l) BWR/6 in Valencia, Spain that was operating at 100% of uprated licensed thermal power for the period in which the current data were taken. Cofrentes was uprated 2% in 1988, another 2.2% in 1998, 5.6% in 2002 and 1.9% in 2003, taking it to 112% of original capacity.

The rated power in the original design was 2894 MWt. The original power density was 52 kW/l. The current licensed power level is 3238 MWt thus represents a 11.9% up-rate. The cycle 15 core was composed of a heterogeneous loading of multiple fuel types from multiple vendors, including GE12, SVEA-96, OPTIMA2 and GE14 product lines. The GE product lines include part length rods. Contrary to common industry practice, fuel products from multiple vendors are loaded simultaneously. For purposes of establishing the correct isotopic history, the Cofrentes core has been tracked from initiation of Cycle 5 (1989).

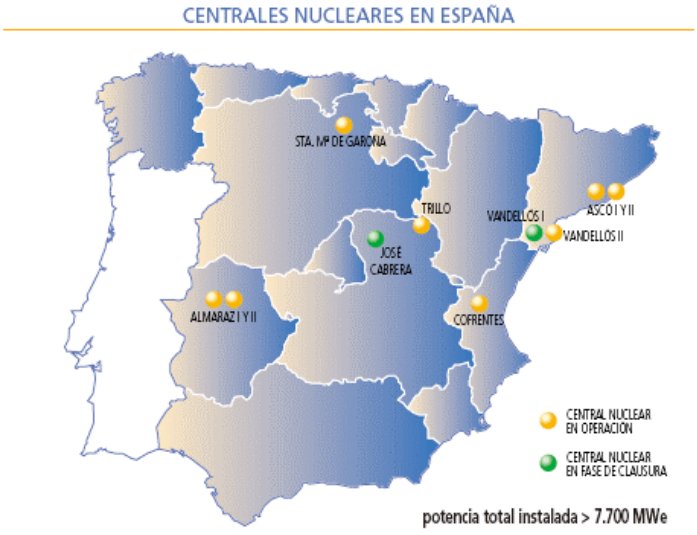

4.1 CYCLE 15A OPERATION

Cycle 15A started on 10/16/2003 and ended 05/01/2004. The inventory of fuel in the core is provided in Table 4-1. A map of the bundle ID's is provided in Figure 4-1. The location of the fifty bundles that were gamma scanned at EOC15B is provided in Figure 4-2. A series of 26 off-line core-tracking cases deplete the core to the cycle average exposure of [[ ]] MWd/ST at End of Cycle 15A (EOC15A). At the end of the cycle, a ten-day mid cycle outage was taken to replace a leaker fuel assembly. Figure 4-3 provides the power and flow conditions for Cycle 15A. Figure 4-4 provides an indication of the control rod inventory as well as the core average void fraction for Cycle 15A. Figure 4-5 displays the PANAC11 hot core tracking eigenvalue and the peak bundle power in MWt in Cycle 15A.

Table 4-1

Bundle Inventory Cycle 15A (BOC)

Bundle	IAT	# In Core	#Fresh	BOC 15A Avg Exp GWd/ST
[[	1	64	0	[[
	2	64	0	
	3	64	0	
	4	48	0	
	5	72	0	
	6	76	0	
	7	72	72	
	10	56	56	
	11	80	80	
	12	16	0	
]]	13	12	0	]]

[[

]]

Figure 4-1. Core ID Map Cycle 15A

[[

]]

Figure 4-2. Core Bundle Type Map Cycle 15A

[[

]]

Figure 4-3. Power and Flow as a Function of Exposure Cycle 15A

[[

]]

Figure 4-4. Control Rod Notches Inserted and Core Average Void Fraction as a Function of Exposure Cycle 15A

[[

]]

Figure 4-5. PANAC11 Hot Eigenvalue and Peak Bundle Power (MWt) as a Function of Exposure Cycle 15A

4.2 CYCLE 15B OPERATION

Cycle 15B started on 05/11/2004 and ended 05/14/2005. The inventory of fuel in the core is provided in Table 4-2. A map of the bundle ID's is provided in Figure 4-6. Note that no bundles are marked as fresh, since the core is now composed of only exposed fuel assemblies. The location of the fifty bundles that were gamma scanned at EOC15B is provided in Figure 4-7. A series of 45 off-line core-tracking cases deplete the core to the cycle average exposure of [[ ]] MWd/ST at End of Cycle 15B (EOC15B). Thus the complete cycle 15 is modeled with (26 + 45=) 71 core tracking cases, and the total cycle 15 exposure length is [[ ]]MWd/ST.

Figure 4-9 provides the power and flow conditions for Cycle 15B. Figure 4-9 provides an indication of the control rod inventory as well as the core average void fraction for Cycle 15B. Figure 4-10 displays the PANAC11 hot core tracking eigenvalue and the peak bundle power in MWt in Cycle 15B.

For Cycle 15B, TIP comparisons of the off-line non-adapted model with the measured TIPs are provided in Appendix A.

Table 4-2

Bundle Inventory Cycle 15B

Bundle Name	IAT	# In Core	#Fresh	BOC 15B Avg Exp GWd/ST
[[	1	64	0	[[
	2	64	0	
	3	64	0	
	4	47	0	
	5	72	0	
	6	75	0	
	7	72	0	
	10	56	0	
	11	80	0	
	12	18	0	
]]	13	12	0	]]

[[

]]

Figure 4-6. Core ID Map Cycle 15B

[[

]]

Figure 4-7. Core Bundle Type Map Cycle 15B

[[

]]

Figure 4-8. Power and Flow as a Function of Exposure Cycle 15B

[[

]]

Figure 4-9. Control Rod Notches Inserted and Core Average Void Fraction as a Function of Exposure Cycle 15B

[[

]]

Figure 4-10. PANAC11 Hot Eigenvalue and Peak Bundle Power (MWt) as a Function of Exposure Cycle 15B

5. DESCRIPTIONS OF GAMMA SCAN BUNDLES

This section provides descriptions and details of the fifty (50) bundles that were gamma scanned during the outage at EOC15B.

5.1 BWREDB BUNDLE NUMBER

Within the GE nuclear analysis system, bundle designs are identifiable by the BWREDB number (BNUMB). Table 5-1 provides the correspondence between the bundle names and the bundle numbers for the Cofrentes fuel in Cycle 15B.

Table 5-1

Bundles

IAT	BNUMB	Description
1	3807	[[
2	3806	
3	3852	
4	2479	
5	2478	
6	2550	
7	2625	
10	3056	
11	3057	
12	3807	
13	3806	]]

5.2 LIST OF BUNDLES

Table 5-2 provides a list of the bundles that were gamma scanned. There are four different product lines. There were 13 OPTIMA2 bundles, 12 GE14 bundles, 10 GE12 bundles, and 15 SVEA96 bundles gamma scanned. A yellow background notes the four bundles for which the gamma scan measurements were in error; these fuel assemblies are deleted from all further tables, figures, and discussions. This leaves 13 OPTIMA2 bundles, 12 GE14 bundles, 8 GE12 bundles, and 13 SVEA96 bundles in the gamma scan database.

Table 5-2

List of 50 Bundles Gamma Scanned

#	OPTIMA2	GE14	GE12	SVEA96
1	[[			
2				
3				
4				
5				
6				
7				
8				
9				
10				
11				
12				
13				
14				
15				]]

5.2.1 Core Locations and EOC15B Bundle Average Exposures

Table 5-3 provides the core position (in site coordinates), bundle type (IAT type), and EOC15B bundle average exposure for the forty-six gamma scanned bundles in the final database. The distance from the center of the core is presented in units of 'nodes'. Each node represents a distance of six inches. This information on exposures and nodal distances is used in Figures 9-2, 9-3, 9-5, and 9-6.

Table 5-3

Core location, Bundle Type, and Bundle Average Exposure

Count	Fuel_ID	Type	IAT Type	Core_pos	PANAC I	PANAC J	Bundle Avg Exposure GWd/ST	Distance From Center Of Core
1	[[	.....						
2		.....						
3		.....						
4		.....						
5		.....						
6		.....						
7		.....						
8		.....						
1		.....						
2		.....						
3		.....						
4		.....						
5		.....						
6		.....						
7		.....						
8		.....						
9		.....						
10		.....						
11		.....						
12		.....						
1		.....						
2		.....						
3		.....						
4		.....						

Count	Fuel_ID	Type	IAT Type	Core_pos	PANAC I	PANAC J	Bundle Avg Exposure GWd/ST	Distance From Center Of Core
5		.....						
6		.....						
7		.....						
8		.....						
9		.....						
10		.....						
11		.....						
12		.....						
13		.....						
1		.....						
2		.....						
3		.....						
4		.....						
5		.....						
6		.....						
7		.....						
8		.....						
9		.....						
10		.....						
11		.....						
12		.....						
13		.....						]]

6. CHARACTERIZATION OF OPERATING CONDITIONS - GAMMA SCAN BUNDLES

The prior operating history of the bundles that were gamma scanned is of interest. This section provides some additional details regarding the operating conditions seen in Cycles 15A and 15B. All information in this section is obtained from the off-line non-adapted PANAC11 core tracking cases.

6.1 KEY OPERATING PARAMETERS

The Safety Evaluation (SE) by the NRC that covers the Licensing Topical Report NEDC-33173P, "Applicability of GE Methods to Expanded Operating Domains," Reference [8], discusses "Key Operating Parameters" in Section 2.1.1. A portion of this section is paraphrased below.

6.1.1 Section 2.1.1 of SE

The core thermal-hydraulic conditions for operation at EPU and MELLLA+ can be measured by review of the following key parameters:

(1) Power of Peak Bundle

The bundle power (in MW) is a fundamental direct input to the critical power ratio (CPR) safety parameter calculation, the linear heat generation rate (LHGR), the initial conditions for loss-of-coolant accident (LOCA) response, and the calculation of other intermediate quantities. It represents a local metric of operating conditions and is relevant particularly to the performance of the steady-state nuclear methods.

(2) Coolant Flow for Peak Bundle

The active bundle flow (in Mlbm/hr) is also a direct input to the calculation of the CPR safety parameter, as well as other intermediate quantities.

(3) Exit Void Fraction for Peak Power Bundle

The void fraction results from the integration of the bundle power and flow, as well as the axial distribution of power deposition along the bundle.

(4) Maximum Channel Exit Void Fraction

The peak power bundle (hot channel) may not always coincide with the bundle with the highest channel exit void fraction, since this parameter is based not only on total bundle power, but also on bundle flow.

(5) Core Average Exit Void Fraction

The core average exit void fraction is a core-wide metric on the amount of heat being carried by the coolant.

(6) Peak LHGR

The peak LHGR (in kW/ft) is a reasonable measure of degree of peaking in the core since it is comprised of the combination of radial, axial, and local (pin) power peaking. It is also a key design constraint and monitoring parameter.

(7) Peak Nodal or Pin Exposure

The nodal and pellet exposures are determined by integration of the energy extracted from the local physical area of the fuel given its original specific mass.

6.2 CHARACTERIZATION OF OPERATING CONDITIONS - GAMMA SCAN BUNDLES

The purpose for this section is to characterize some of the operating parameters for the bundles used in the Cofrentes 2005 gamma scan. The following information is based on the non-adapted off-line core tracking.

- Figure 6-1 provides information regarding the bundle power (expressed in MWt) as a function of cycle exposure in Cycle 15B for the maximum of each of the four bundle types.
- Figure 6-2 provides information regarding the bundle flow in lb/hr as a function of cycle exposure in Cycle 15B for the maximum of each of the four bundle types.
- Figure 6-3 provides the ratio of the core power in MWt / Total Core Flow in Mlb/hr as a function of exposure in Cycle 15B. As can be seen, the maximum value is [[ ]].
- Figure 6-4 provides information regarding the peak nodal exposure (in MWd/ST) vs. Cycle exposure (in MWd/ST).
- Figure 6-5 provides information regarding the ratio (bundle power in MWt) / (bundle flow in lb/hr) as a function of cycle exposure in Cycle 15B for the maximum of each of the four bundle types.
- Figure 6-6 provides information regarding the average void fraction as a function of cycle exposure in Cycle 15B for the maximum of each of the four bundle types.
- Figure 6-7 provides information regarding the exit void fraction as a function of cycle exposure in Cycle 15B for the maximum of each of the four bundle types.
- Figure 6-8 provides information regarding the bundle peak Linear Heat Generation Rate (LHGR) in kW/ft as a function of cycle exposure in Cycle 15B for the maximum of each of the four bundle types.
- Figure 6-9 provides information regarding the control rod insertion as a function of cycle exposure in Cycle 15B for the nine gamma scanned bundles that had a control rod adjacent to the bundle for any portion of Cycle 15B.

[[

]]

Figure 6-1. Maximum Bundle Power in MWt vs. Cycle 15B Exposure

[[

]]

Figure 6-2. Maximum Flow vs. Cycle 15B Exposure

[[

]]

Figure 6-3. Core Power / Core Flow (MWt/Mlb/hr) vs. Cycle 15B Exposure

[[

]]

Figure 6-4. Peak Nodal Exposure vs. Cycle 15B Exposure

[[

]]

Figure 6-5. Maximum Ratio Bundle Power / Bundle Flow vs. Cycle 15B Exposure

[[

]]

Figure 6-6. Maximum Bundle Average Void Fraction vs. Cycle 15B Exposure

[[

]]

Figure 6-7. Maximum Bundle Exit Void Fraction vs. Cycle 15B Exposure

[[

]]

Figure 6-8. Maximum Bundle kW/ft vs. Cycle 15B Exposure

[[

]]

Figure 6-9. Notch Position Adjacent to Gamma Scan Bundles vs. Cycle Exposure

6.3 EOC15B INFORMATION

The following plots provide insights as to the core average axial exposure, core average axial power, and core average axial void fractions seen at EOC15B from the non-adapted core tracking:

- Figure 6-10. EOC15B Core Average Axial Exposures
- Figure 6-11. EOC15B Core Average Axial Powers
- Figure 6-12. EOC15B Core Average Axial Void Fractions

[[

]]

Figure 6-10. EOC15B Core Average Axial Exposure

[[

]]

Figure 6-11. EOC15B Core Average Axial Power

[[

]]

Figure 6-12. EOC15B Core Average Axial Void Fraction

6.4 Adapted Core Tracking

As will be described in Section 8, in the calculation of the ^{140}Ba distributions, it is necessary to integrate the nodal powers from the PANAC11 core tracking over the last 60 to 120 days of operation. In addition, this is done for both non-adapted and adapted core tracking.

In the adapted core tracking, measured TIP and LPRM data is input into the off-line PANAC11 core tracking model. This data is then used in the same manner as is done in the on-line non-adapted 3DM based core tracking.

For the Cofrentes 2005 Gamma Scan comparisons, TIP and LPRM adapted core tracking was used from [[ ]]. This corresponds to a cycle exposure interval from [[ ]].

6.4.1 Comparisons of Adapted and Non-Adapted Core Average Axial Power Shapes

Figure 6-13 provides the core average axial power shape from the off-line non-adapted core tracking for the cases used to integrate the ^{140}Ba distributions. The TIP and LPRM adapted power shapes for these same cases are given in Figure 6-14. A comparison of the non-adapted and adapted core average axial power shapes is provided in Figure 6-15.

[[

]]

Figure 6-13. Core Average Axial Powers from 6322 MWd/ST to EOC for Non-Adapted Core Tracking

[[

]]

Figure 6-14. Core Average Axial Powers from 6322 MWd/ST to EOC for TIP and LPRM Adapted Core Tracking

[[

]]

Figure 6-15. EOC15B Core Average Axial Power Comparisons

7. BUNDLE MEASUREMENT DATA

7.1 MEASUREMENT DETAILS

The measurement process for the 50 fuel assemblies described in Section 3 were made at 25 axial elevations for each of the 50 fuel assemblies. At each axial elevation, eight (8) measurements were made, two at each corner of the fuel assembly. During the measurement campaign, repeat measurements were made of the same fuel assembly to ensure that the measurement systems continued to be properly calibrated. Following the measurements, a decay correction was applied to bring the ^{140}La values back to the time of the actual shutdown. This time corrected ^{140}La value was then normalized such that the average of all readings was 1.0.

7.2 DATA UNCERTAINTY AND DATA ELIMINATION

Nodes 1 and 23-25 were excluded from the normalization as they have generally larger uncertainties caused by external objects hindering the measurements. As reported by the experimental group that made the measurements, the experimental uncertainties were estimated to be [[ ]].

7.3 GAMMA SCAN DATA

The gamma scan measurement data is summarized in Figures 7-1 through 7-5 as follows:

- Figure 7-1 contains the measured normalized Gamma Scan measurement data for all fifty of the fuel assemblies.
- Figure 7-2 contains the measured normalized Gamma Scan measurement data for the GE12 Fuel Assemblies.
- Figure 7-3 contains the measured normalized Gamma Scan measurement data for the GE14 Fuel Assemblies.
- Figure 7-4 contains the measured normalized Gamma Scan measurement data for the OPTIMA2 Fuel Assemblies.
- Figure 7-5 contains the measured normalized Gamma Scan measurement data SVEA96 Fuel Assemblies.

[[

]]

Figure 7-1 Gamma Scan Measurement Data for All Fuel Assemblies

[[

]]

Figure 7-2 Gamma Scan Measurement Data for GE12 Fuel Assemblies

[[

]]

Figure 7-3 Gamma Scan Data for GE14 Fuel Assemblies

[[

]]

Figure 7-4 Gamma Scan Measurements for OPTIMA2 Fuel Assemblies

[[

]]

Figure 7-5 Gamma Scan Measurements for SVEA96 Fuel Assemblies

8. GAMMA SCAN COMPARISON OVERVIEW

8.1 UTILIZATION OF THE DATA FOR POWER DISTRIBUTION BENCHMARK

The gamma scanning technique measures the 1.596 MeV gamma ray that accompanies the beta decay of ^{140}La. The primary mechanism for the accumulation of ^{140}La in exposed fuel is the beta decay of the fission product ^{140}Ba with a half-life of 12.79 days. Because of this equilibrium time constant, the ^{140}Ba distribution is characteristic of the integrated power history of the core during the last 2 to 3 months before shutdown.

Since the half-life of ^{140}La, 40.23 hours, is much shorter than that of, ^{140}Ba, following a period of approximately 10 days after shutdown, the ^{140}La activity is decaying at a rate determined by the half-life of ^{140}Ba and is proportional to the ^{140}Ba atom density.

The relationship between the production rate of ^{140}Ba (S_B) and fission density (F), at a time t, is given by

$$S_B = \left\{ \sum_k Y_{Bk} f_k \right\} F \quad , \quad \frac{Barium\ atoms}{cm^3 \sec}$$

where

Y_{Bk} = cumulative fission yield of Ba-140 from fissile nuclide k

f_k = fraction of fissions for fissile nuclide k

In the case of most fuels under consideration, the number of fissile nuclides, k, which contribute significantly to the fission rate, is small. Thus, we use

$$Y_e = effective\ yield = \sum_{k=1}^{4} Y_k f_k \Big/ \sum_{k=1}^{4} f_k \ , k = U-235, U-238, Pu-239\ and\ Pu-241$$

To determine the total accumulation of Ba-140, then, requires solving the equation

$$\frac{dN_B(t)}{dt} = Y_e F(t) - \lambda_B N_B(t) \quad ,$$

where

N_B = Ba-140 atom density, atoms/cm^3

λ_B = Ba-140 decay constant = 0.05419 day^{-1}

Assuming that F is stepwise constant over the interval $\Delta t = t_n - t_{n-1}$ and equals to the average, therefore replacing the time integral with successive substitution, as

$$N_B(t_n) = \frac{Y_e(t_n)F(t_n)}{\lambda_B} + \left[N_B(t_{n-1}) - \frac{Y_e(t_n)F(t_n)}{\lambda_B} \right] \exp(-\lambda_B \Delta t) \quad .$$

8.2 CONSIDERING GEOMETRICAL EFFECTS ON THE GAMMA SCAN

The measured gamma scan data supplied to GNF consists of nodal average values of measured detector signal intensity (pulses) of the 1596 keV gamma ray resulting from decay of ^{140}La. Each bundle was measured twice on all four corners for a total of eight measurements. These measurements were averaged together to determine the "node" value. The transmittal indicates that all measurement corrections (detector dead-time, drift, extent of measurements, etc.) have been applied. The detector intensity was provided in arbitrary units consistent for all assemblies. Figure 8-1 shows the general geometry of the gamma scan system.

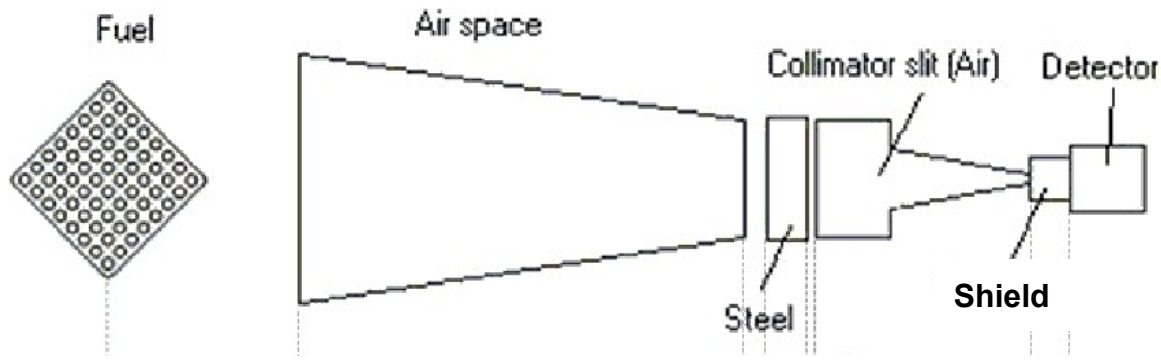

Figure 8-1 Depiction of the fuel and collimator geometry

Because the lattices in these bundles were of differing type with differing water and part length rod locations, the geometric and material difference between each lattice type must to be taken into account when trying to normalize the collimator response to the 1596 keV ^{140}La gamma rays. The problem is analogous to geometric view factors used for radiative heat transport calculations. The MCNP Monte Carlo neutron transport code was used to simulate the explicit geometry for the purpose of characterizing the lattices on a relative basis. The gamma ray source terms for this simulation were taken from TGBLA06 pin power distributions for the nodal exposure and spectral history calculated by PANAC11. These correction (or inter-calibration) factors were used to re-normalize the measured collimator responses for the purpose of comparing the nodal simulator predictions to the measurements. However, this operation should not be considered experimental correction but rather another component of the GNF analytical methodology prediction process.

8.2.1 Cofrentes 2005 Geometric Correction Factors

Because these geometric correction factors depend to some extent on the gamma ray source distributions within the fuel, it was necessary to calculate new correction factors for the specific fuel assemblies gamma scanned in this campaign. This section documents these geometric correction factors in Figures 8-2 through 8-5.

[[

]]

Figure 8-2 GE12 Geometric Correction Factors

[[

]]

Figure 8-3 GE14 Geometric Correction Factors

[[

]]

Figure 8-4 OPTIMA2 Geometric Correction Factors

[[

]]

Figure 8-5 SVEA96 Geometric Correction Factors

8.3 DEFINITION OF STATISTICS AND PROCESS

The definition of the appropriate statistical population recognizes two important elements. First, bundles are often grouped by region, IAT, or complete four-bundle cell. Second, the measured data had higher uncertainties on the lowest and two highest nodes.

Measured and simulated data are normalized as follow:

$$\tilde{G}_k^n = G_k^n * \frac{\sum_{n=1}^{N} W(n) * K}{\sum_{n=1}^{N} \sum_{k=Klow}^{Kup} G_k^n * W(n)}$$

where,

G : raw barium density (measured or simulated)

$\tilde{G}$: normalized barium density (measured or simulated)

k : axial elevation index

n : scanned bundle index

N : total number of scanned bundles

Klow : minimum axial elevation used in the statistics

Kup : maximum axial elevation used in the statistics

K = Kup – Klow + 1

W(n) : weighting =1 if octant interior bundle without symmetric pairs in the gamma scan database

= 0.5 if bundle is on a diagonal

= 1/L if bundle has L other symmetric bundles in the gamma scan database

The default option in the normalization process is to use the "octant" weighting option (=0), with the coefficients W(n) described above. The alternative is to use uniform weighting for every bundle (weighting option =1).

The bundle average data is calculated as follow:

$$G_b^n = \frac{\sum_{k=Klow}^{Kup} \tilde{G}_k^n}{K}$$

If g_{nk} denotes the gamma scan data, p_{nk} denotes the simulator prediction for bundle n and node k, while N defines the set of appropriate bundles, "SIGMA" and "RMS" denote the following relationship for nodal statistical comparisons.

$$d_{nk} = p_{nk} - g_{nk}$$

$$\bar{D} \equiv \frac{1}{K * N} \sum_{n=1}^{N} \sum_{k=Klow}^{Kup} d_{nk}$$

$$SIGMA = \sigma = \sqrt{\frac{1}{K * N - 1} \sum_{n=1}^{N} \sum_{k=Klow}^{Kup} (d_{nk} - \bar{D})^2}$$

$$RMS = \sqrt{\frac{1}{K * N} \sum_{n=1}^{N} \sum_{k=Klow}^{Kup} (p_{nk} - g_{nk})^2}$$

For nodal comparisons, the p_{nk} and g_{nk} denote nodal values over the valid axial positions (K_{low} to K_{up}) for bundles defined in the set. For bundle comparisons, a similar statistic is created were the delta is based upon difference between the average values from the valid axial positions for all bundles defined in the set.

For axial comparisons, the comparison is exactly the same as the nodal comparison except that the bundle average bias is first normalized away for each fuel assembly so that the axial shape may be isolated and compared. In the comparisons provided herein, the axial RMS is evaluated after normalization of each fuel assembly to a radial power of 1.0 for each fuel assembly. Note that this is a slight change compared to the process used for the Cofrentes 2002 Gamma Scan evaluation.

A description of the [[ ]] statistic is contained in Section 10.

9. DESIGN CALCULATIONS

This document provides summaries of the comparisons of design calculations of ^{140}Ba with measured ^{140}La as a means of demonstrating the GNF capabilities for calculating nodal powers. There are two analytic approaches summarized herein for predicting the nodal ^{140}Ba. These include:

- The standard off-line TGBLA06 / PANAC11 non-adapted models used in GNF applications for reload design and licensing (non-adapted off-line);
- The standard on-line TGBLA06 / PANAC11 application used in 3DMonicore™ with TIP and LPRM shape adaptation for on-line monitoring (adapted off-line).

For both of these analytic approaches, the nodal power distributions from the PANAC11 core tracking are post processed to produce the nodal ^{140}Ba distributions as described in Section 4.1 of NEDC-33173P, Supplement 1, Part 1. (Power Distribution Validation for Cofrentes Cycle 13, Reference [4]).

9.1 STATISTICAL COMPARISONS

Comparisons between the (normalized) predicted ^{140}Ba distributions with the (normalized) measured ^{140}La distributions demonstrate that the uncertainties in the predictions are significantly less than the uncertainties used for pin-by-pin power distributions in the GNF calculation process used in support of licensing calculations.

9.2 BUNDLE ELIMINATIONS

As mentioned, there were fifty (50) bundles that were gamma scanned during the outage at EOC15B. There were four bundles for which the gamma scan measurements were in error (a required additional absorber in the beam was missing). These four bundles are identified in Table 9-1. In the discussion in this chapter, statistical comparisons will be provided for three different groupings of the 46 remaining bundles: (a) all bundles, (b) eliminating two bundles on the periphery, and (c) eliminating two peripheral and three near peripheral bundles. [[

]] The bundles eliminated for each of these groupings are also identified in Table 9-1.

Table 9-1 Summary of Bundles Eliminated

Case	Number of Bundles Analyzed	Bundles Eliminated			
Four operator error bundles removed	46	[[			
Two peripheral bundles removed	44				
3 near peripheral bundle removed	41				]]

9.3 SUMMARY OF BUNDLE / AXIAL / NODAL COMPARISONS

Table 9-2 summarizes statistical comparisons for the bundle, axial, and nodal components for the PANAC11 model. In these comparisons, only nodes 2-22 are considered.

The first three rows of data provide results when all 46 Gamma Scan fuel assemblies are included in the comparison. Eliminating two bundles on the outer peripheral locations results in only 44 fuel assemblies, as shown in the next two rows of Table 9-1. Eliminating three additional near peripheral fuel assemblies results in only 41 fuel assemblies in the database.

Table 9-2 Summary of Bundle / Axial / Nodal Comparisons

Core Tracking	Weighting	Number of Bundles	Bundle RMS	Bundle SIGMA	Axial RMS	Axial SIGMA	Nodal RMS	Nodal SIGMA	Case
Non-adapted	Octant	46	[[						Four Operator Error Bundles Removed
Non-adapted	Unit	46							Four Operator Error Bundles Removed
TIP and LPRM Adapted	Unit	46							Four Operator Error Bundles Removed
Non-adapted	Unit	44							Two Peripheral Bundles Removed
TIP and LPRM Adapted	Unit	44							Two Peripheral Bundles Removed
Non-adapted	Unit	41							3 near peripheral and 2 peripheral Removed
TIP and LPRM Adapted	Unit	41						]]	3 near peripheral and 2 peripheral Removed

Note that the adaption process has almost no affect on the radial comparison statistics, and that only slight improvements in the radial RMS are seen when peripheral or near peripheral bundles are eliminated.

As documented in Section 7.2, the experimental uncertainties are on the order of [[ ]] Thus the differences between the adapted and non-adapted nodal RMS values are well within the statistical uncertainty of the measurements.

9.4 COMPARISON OF BUNDLE INTEGRAL MEASURED ^{140}LA VS. PREDICTED ^{140}BA – NON-ADAPTED

In Figure 9-1 the plot cross plots the measured ^{140}La against the predicted ^{140}Ba from the PANAC11 core tracking. This data includes the peripheral bundles for the non-adapted core tracking.

[[

]]

Figure 9-1 Plot Bundle Average Measured ^{140}La vs. Predicted ^{140}Ba – Non-Adapted

As can be seen, the predicted and measured bundle integrated values are remarkably consistent over a wide range of bundle powers.

In an effort to discern trends in this data, the variation of this data with other parameters could be examined. The following plots provide some examples of insights that can be gained.

Figure 9-2 plots the same data vs. the distance from the center of the core (the radial nodes are separated by six inches; the unit of measure for the plots is distance in nodes, which is exactly equivalent to bundles.) As can be seen, the two bundles with the largest error are directly on the periphery of the core. These bundles do not contribute to the SLMCPR calculation, as their powers are much too low (These radial powers are on the order of 0.30).

[[

]]

Figure 9-2 Plot Ratio { (Predicted / Measured) –1 } vs. Distance from Center of Core - Non-Adapted

Figure 9-3 plots the ratio of the bundle-integrated ^{140}La from the measured data with the bundle integrated predicted ^{140}Ba from the off-line non-adapted PANAC11 core tracking against the bundle average exposure in MWd/ST.

In Figure 9-3, all 46 fuel assemblies are included. While the data for the once burnt lower exposure fuel assemblies is relatively tightly packed, the data for both of the higher exposure bundle types shows more scatter, with no discernable trends with exposure. There are two bundles that have larger errors than the remainder of the fuel assemblies; as mentioned, these two fuel assemblies are directly on the periphery. The predicted value is higher than the measured for these peripheral bundles, perhaps identifying that some slight improvements might be obtained by a re-examination of the radial leakage components in the PANAC11 model.

[[

]]

Figure 9-3 Plot Ratio { (Predicted / Measured) –1 } vs. Bundle Average Exposure – Non-Adapted

9.5 COMPARISON OF BUNDLE INTEGRAL MEASURED ^{140}LA VS. PREDICTED ^{140}BA – TIP AND LPRM-ADAPTED

In Figure 9-4 the plot cross plots the measured ^{140}La against the predicted ^{140}Ba from the TIP and LPRM adapted PANAC11 core tracking. This data includes the peripheral bundles for the TIP and LPRM adapted core tracking.

[[

]]

Figure 9-4 Plot Bundle Average Measured ^{140}La vs. Predicted ^{140}Ba - Adapted

As can be seen, the predicted and measured bundle integrated values are again remarkably consistent over a wide range of bundle powers and not appreciably different from the non-adapted comparison.

In an effort to discern trends in this data, the variation of this data with other parameters could be examined. The following plots provide some examples of insights that can be gained.

Figure 9-5 plots the same data vs. the distance from the center of the core (the radial nodes are separated by six inches; the unit of measure for the plots is distance in nodes, which is exactly equivalent to bundles.) As can be seen, for the TIP and LPRM adapted core tracking case, the two bundles with the largest error are directly on the periphery of the core, just as in the non-adapted results.

These bundles do not contribute to the SLMCPR calculation, as their powers are much too low (These radial powers are on the order of 0.30)

[[

]]

Figure 9-5 Plot Ratio { (Predicted / Measured) –1 } vs. Distance from Center of Core - Adapted

Figure 9-6 plots the ratio of the bundle-integrated ^{140}La from the measured data with the bundle integrated predicted ^{140}Ba from the off-line TIP and LPRM adapted PANAC11 core tracking against the bundle average exposure in MWd/ST.

In Figure 9-6, all 46 fuel assemblies are included. While the data for the once burnt lower exposure fuel assemblies is relatively tightly packed, the data for both of the higher exposure bundle types shows more scatter, with no discernable trends with exposure. There are two bundles that have larger errors than the remainder of the fuel assemblies; as mentioned, these two fuel assemblies are directly on the periphery.

[[

]]

Figure 9-6 Plot Ratio { (Predicted / Measured) –1 } vs. Bundle Average Exposure –Adapted

9.6 COMPARISON OF AXIAL DATA

The Axial RMS values summarized in Table 9-2 demonstrate that only small differences are seen in the axial power shapes when the peripheral and near peripheral bundles are excluded from the statistics. Therefore the comparisons of axial data will focus on the data when all 46 bundles are included. Figure 9-7 provides a comparison of the measured and predicted axial averaged distributions for the case of all 46 bundles, with non-adapted core tracking. For the TIP and LPRM adapted case, the comparison is shown in Figure 9-8. 'GSDATA' refers to measured data, while 'PCDATA' refers to predicted (PANAC11) data.

[[

]]

Figure 9-7 Axial Comparison for All 46 Bundles – Non-adapted Core Tracking

[[

]]

Figure 9-8 Axial Comparisons for All 46 Bundles – TIP and LPRM Adapted Core Tracking

9.7 NODAL SCATTER PLOT COMPARISONS – NON-ADAPTED

Figure 9-9 provides a plot of the nodal measured ^{140}La against the predicted ^{140}Ba from the non-adapted PANAC11 core tracking. All bundle types are shown in Figure 9-4, for all 46 measured fuel assemblies. Figures 9-10 through 9-13 provide this same information for each of the four bundle types. All of the plots in this section use non-adapted core tracking.

[[

]]

Figure 9-9 Plot Nodal Measured ^{140}La vs. Predicted ^{140}Ba – All Bundles Non-Adapted

[[

]]

Figure 9-10 Plot Nodal Measured ^{140}La vs. Predicted ^{140}Ba – GE12 Bundles Non-Adapted

[[

]]

Figure 9-11 Plot Nodal Measured ^{140}La vs. Predicted ^{140}Ba – GE14 Bundles Non-Adapted

[[

]]

Figure 9-12 Plot Nodal Measured ^{140}La vs. Predicted ^{140}Ba - SVEA96 Bundles Non-Adapted

[[

]]

Figure 9-13 Plot Nodal Measured ^{140}La vs. Predicted ^{140}Ba – OPTIMA2 Bundles Non-Adapted

9.8 NODAL SCATTER PLOT COMPARISONS – TIP AND LPRM ADAPTED

Figure 9-14 plots the nodal measured ^{140}La against the predicted ^{140}Ba from the TIP and LPRM adapted PANAC11 core tracking. All bundle types are shown in Figure 9-14, for all 46 measured fuel assemblies. Figures 9-15 through 9-18 provide this same information for each of the four bundle types. All of the plots in this section use TIP and LPRM adapted core tracking.

[[

]]

Figure 9-14 Plot Nodal Measured ^{140}La vs. Predicted ^{140}Ba – All Bundles Adapted

[[

]]

Figure 9-15 Plot Nodal Measured ^{140}La vs. Predicted ^{140}Ba – GE12 Bundles Adapted

[[

]]

Figure 9-16 Plot Nodal Measured ^{140}La vs. Predicted ^{140}Ba – GE14 Bundles Adapted

[[

]]

Figure 9-17 Plot Nodal Measured ^{140}La vs. Predicted ^{140}Ba - SVEA96 Bundles Adapted

[[

]]

Figure 9-18 Plot Nodal Measured ^{140}La vs. Predicted ^{140}Ba – OPTIMA2 Bundles Adapted

9.9 AXIAL TRENDING VS AXIAL HEIGHT

Figure 9-19 uses the nodal data and compares the difference Measured minus Predicted (GSNORM-PCNORM) for non-adapted core tracking comparisons (with unit weighting for 46 fuel assemblies, peripheral bundles are excluded). Figure 9-20 provides the same comparison for the TIP and LPRM adapted core tracking. Both plots include the average delta, and error bars at a one sigma value.

[[

]]

Figure 9-19 Examination of Trending vs. Axial Height - Non-adapted (All Bundles)

[[

]]

Figure 9-20 Examination of Trending vs. Axial Height – Adapted (All Bundles)

9.9.1 Axial Trending for Non-Adapted Core Tracking

This section focuses on the axial trending for only the non-adapted core tracking, providing different views for both the delta difference between the measured and predicted values, as well as the ratio of measured / predicted. Figure 9-21 provides information regarding the difference between measured and predicted, presented as the average for all fuel, and for each of the difference bundle types, while Figures 9-22 through 9-25 provide more detailed information for each fuel type.

[[

]]

Figure 9-21 Axial Plot Delta Measured minus Predicted by Fuel Type - Non-adapted

[[

]]

Figure 9-22 Axial Plot Delta Measured minus Predicted For GE12 - Non-adapted

[[

]]

Figure 9-23 Axial Plot Delta Measured minus Predicted For GE14 - Non-adapted

[[

]]

Figure 9-24 Axial Plot Delta Measured minus Predicted For OPTIMA2 - Non-adapted

[[

]]

Figure 9-25 Axial Plot Delta Measured minus Predicted For SVEA96 - Non-adapted

Figure 9-26 uses the nodal data and compares the ratio Measured / Predicted (GSNORM / PCNORM) for non-adapted core tracking comparisons (with unit weighting for 46 fuel assemblies, peripheral bundles are excluded). Equivalent trends to the presentation of the difference between measured and predicted in Figure 9-19 are evident.

[[

]]

Figure 9-26 Axial Plot Delta Measured / Predicted All Fuel - Non-adapted

9.10 RADIAL COMPARISON MAP

Figure 9-21 provides additional detail on the radial comparisons for all forty-six bundles (data is non-adapted unit weighting).

[[

]]

Figure 9-21 Radial Comparison Data

10. [[ ]]

10.1 DEFINITION OF STATISTICS

As described in the SLMCPR methodology, a gamma scan affords insight into the [[

]]. The difference between the bundle prediction and measurement yields this insight. This particular uncertainty has been the subject of recent communications with the NRC.

In each four-bundle set, the [[ ]]is computed as

[[

]]

where P_j is the bundle-integrated ^{140}Ba for bundle j. Therefore, in terms of the normalized gamma scan data or prediction,

[[

]]

10.2 [[ ]] SUMMARY

The summary of [[ ]] is provided in Table 10-1.

Table 10-1 Summary of [[ ]] Statistics

Core Tracking	Weighting	Number of Bundles	Number of 4 Bundle Sets	RMS	SIGMA	Note
Non-adapted	Octant	46	9	[[		Four Operator Error Bundles Removed
Non-adapted	Unit	46	9			Four Operator Error Bundles Removed
TIP and LPRM Adapted	Unit	46	9			Four Operator Error Bundles Removed
Non-adapted	Unit	44	8			Two Peripheral Bundles Removed
TIP and LPRM Adapted	Unit	44	8			Two Peripheral Bundles Removed
Non-adapted	Unit	41	8			3 near peripheral and 2 peripheral Removed
TIP and LPRM Adapted	Unit	41	8		]]	3 near peripheral and 2 peripheral Removed

10.3 [[ ]] DIFFERENCES

Figures 10-1 and 10-2 provide comparisons for the [[ ]] differences for the cases with 44 fuel assemblies (non-adapted and adapted core tracking, respectively). The peripheral and near-peripheral bundles are excluded as they would not contribute in the SLMCPR calculation process (bundle powers are too low).

[[

]]

Figure 10-1 [[ ]] **- 44 Bundles Non-Adapted**

[[

]]

Figure 10-2 [[ ]] **Differences Adapted - 44 Bundles**

11. CONCLUSIONS

The power distribution validation data for Cofrentes Cycle 15 is quite comparable to the Cofrentes Cycle 13 data (Reference 4). These results are consistent with the original SLMCPR analysis, and hence confirm that no changes to the SLMCPR uncertainties are needed for modern core and fuel designs or operational strategies. Considering the uncertainties derived from the data examined to date with the TGBLA06/PANAC11 methodology, the power distributions uncertainties could be reduced from the current values applied in the SLMCPR analysis.

In comparing the results for non-adapted and adapted core tracking, the data in this document also supports the contention that on-line non-adapted 3DM PANAC11 based monitoring is statistically equivalent to adapted 3DM PANAC11 based monitoring.

11.1 SUMMARY OF BUNDLE AND NODAL COMPARISONS

The results between the measurements and predictions using the TGBLA06 lattice physics code and the PANAC11 BWR core simulator are excellent. Table 11-1 compares the bundle and nodal RMS values for the PANAC11 vs. Gamma Scan measurements for Cycles 13 and 15.

Table 11-1 Summary of Bundle and Nodal RMS Comparisons to Gamma Scan Data

Cycle, Type	Bundle RMS	Nodal RMS
Cycle 13, Non-Adapted	[[	
Cycle 13 Adapted		
Cycle 15 Non-Adapted		
Cycle 15 Adapted		]]

These results are consistent with routinely taken TIP measurements.

Table 11-2 compares the TIP statistics for the TIP sets taken at the Cycles 13 and 15.

Table 11-2 Summary of Non-Adapted PANAC11 to TIP Data at EOC

Cycle, Type	Bundle RMS	Nodal RMS
Cycle 13, Non-Adapted	[[	
Cycle 15 Non-Adapted		]]

These results support the contention that while gamma scan campaigns yield information not available in the more routinely taken TIP measurements, the two validation data sets are wholly consistent.

11.2 SUMMARY OF GAMMA SCAN [[ ]] MEASUREMENTS USING THE PANAC11 3D SIMULATOR

A composite summary of Gamma Scan Measurement comparisons for [[ ]] using the PANAC11 3D simulator is provided in Table 11-3.

Table 11-3 Summary of Gamma Scan Measurements Using the PANAC11 3D Simulator

Plant and Cycle	[[ ]] RMS Difference (%)	Number of 4 Bundle Sets	New Fuel Geometry	Core Power Level (MWt)	Avg. Power Density (kW/l)	New Fuel Batch Fraction
Hatch 1 EOC1	[[	24	7x7	2436 (100%)	51.2	Initial core
Hatch 1 EOC3		26	8x8 (C2) 8x8R (C3)	2436 (100%)	51.2	92 (C2) 168 (C3)
Weighted Average						
Cofrentes EOC13		8	9x9 10x10 SVEA	2891 (100%)	52.4	64 (GE12) 128 (SVEA)
Weighted Average						
Cofrentes EOC15		8	10x10 GE14 10x10 OPTIMA2	3238 (100%)	58.6	72 (GE14) 136 (OPTIMA2)
Weighted Average	]]					

Thus, these comparisons clearly confirm the adequacy of the [[ ]] currently defined in NEDC-32601P-A.

12. REFERENCES

1. Letter from USNRC to G. A. Watford (GE), "Amendment 26 to GE Licensing Topical Report NEDE-24011-P-A, 'GESTAR II' - Implementing Improved GE Steady-State Methods," November 10, 1999.
2. GE Nuclear Energy, “Power Distribution Uncertainties for Safety Limit MCPR Evaluations,” NEDC-32694P-A, August 1999.
3. GE Nuclear Energy, “Advanced Methods Power Distribution Uncertainties for Core Monitoring,” NEDC-32773P, Revision 1, January 1999.
4. GE Hitachi Nuclear Energy, NEDC-33173P, Supplement 2 Part 1, Licensing Topical Report, Applicability of GE Methods to Expanded Operating Domains – Power Distribution Validation for Cofrentes Cycle 13, August 2009.
5. GE Nuclear Energy, “Methodology and Uncertainties for Safety Limit MCPR Evaluations,” NEDC-32601P, December 1996.
6. GE Nuclear Energy, Letter, J. S. Post to NRC, Document Control Desk, “Part 21 Evaluation; Power Distribution Uncertainty Reassessment,” MFN 05-082, August 18, 2005.
7. GE Nuclear Energy “Applicability of GE Methods to Expanded Operating Domains” NEDC-33173P,” February 2006.
8. Letter from TB Blount (NRC) to JG Head (GEH), Subject: Final Safety Evaluation for GE Hitachi Nuclear Energy Americas, LLC Licensing Topical Report NEDC-33173P, “Applicability Of GE Methods To Expanded Operating Domains” (TAC No. MD0277), July 21, 2009.

Appendix A OFF-LINE NON-ADAPTED TIP COMPARISONS

The definitions of statistics used in these TIP comparisons are provided in Reference 4.

A.1 CYCLE 15B NON-ADAPTED TIP SETS

There were eleven TIP sets run during cycle 15B. One of these was run at very low exposure under non-equilibrium Xenon conditions. The off-line core tracking near this point was done only with equilibrium Xenon, which invalidates the off-line TIP comparison, so this case is eliminated from this report. The remaining ten cases are summarized in Table A.1-1 and Figure A.1-1.

A.2 CYCLE 15B - COMPARISON OF CORE AVERAGE AXIAL TIPS – NON-ADAPTED

This subsection provides snapshots of the comparison of the measured and calculated core average axial TIPs at the ten exposure points in Cycle 15B. The progression from a more bottom peaked power distribution at the middle of cycle to a more top peaked power distribution at the end of cycle can be inferred from the core average axial TIP plots.

Table A.1-1

Cycle 15B Non-Adapted TIP Sets

Case	Qualifier	Cycle Exposure MWd/ST	RP MW(t)	WCT Mlbm/hr	Bundle Non-Adapted TIP RMS	Axial Non-Adapted TIP RMS	Nodal Non-Adapted TIP RMS	Core Avg. Ex. Void	Max. Exit Void
1	BJ115D29	[[							
2	BJ115D34								
3	BJ115D39								
4	BJ115D43								
5	BJ115D49								
6	BJ115D53								
7	BJ115D58								
8	BJ115D63								
9	BJ115D68								
10	BJ115D71								
	RMS								
	Mean								
	St. Deviation								
	Minimum								
	Maximum								]]

[[

]]

Figure A.1-1. Cycle 15B TIP RMS Values

[[

]]

Figure A.2-1. Axial Average TIP Comparison at 438 MWd/ST

[[

]]

Figure A.2-2. Individual TIP Comparisons At 438 MWd/ST

[[

]]

Figure A.2-3. Axial Average TIP Comparison at 1545 MWd/ST

[[

]]

Figure A.2-4. Individual TIP Comparisons At 1545 MWd/ST

[[

]]

Figure A.2-5. Axial Average TIP Comparison at 2569 MWd/ST

[[

]]

Figure A.2-6. Individual TIP Comparisons At 2569 MWd/ST

[[

]]

Figure A.2-7. Axial Average TIP Comparison at 3461 MWd/ST

[[

]]

Figure A.2-8. Individual TIP Comparisons At 3461 MWd/ST

[[

]]

Figure A.2-9. Axial Average TIP Comparison at 4764 MWd/ST

[[

]]

Figure A.2-10. Individual TIP Comparisons At 4764 MWd/ST

[[

]]

Figure A.2-11. Axial Average TIP Comparison at 5701 MWd/ST

[[

]]

Figure A.2-12. Individual TIP Comparisons At 5701 MWd/ST

[[

]]

Figure A.2-13. Axial Average TIP Comparison at 6835 MWd/ST

[[

]]

Figure A.2-14. Individual TIP Comparisons At 6835 MWd/ST

[[

]]

Figure A.2-15. Axial Average TIP Comparison at 7835 MWd/ST

[[

]]

Figure A.2-16. Individual TIP Comparisons At 7835 MWd/ST

[[

]]

Figure A.2-17. Axial Average TIP Comparison at 8881 MWd/ST

[[

]]

Figure A.2-18. Individual TIP Comparisons At 8881 MWd/ST

[[

]]

Figure A.2-19. Axial Average TIP Comparison at 9388 MWd/ST

[[

]]

Figure A.2-20. Individual TIP Comparisons At 9388 MWd/S